On Vehicle Pitch Estimation via solid-state LIDAR

Donald Selmanaj [*] **Matteo Corno** [**] **Giulio Panzani** [**]
Sergio M. Savaresi [**]

[*] *Department of Automation, Polytechnic University of Tirana, Sheshi*
"Nënë Tereza", Nr.4, Tirana, Albania (e-mail:
donald.selmanaj@fie.upt.al).
[**] *Dipartimento di Elettronica, Informazione e Bioingegneria,*
Politecnico di Milano, Piazza L. da Vinci, 32, 20133, Milano, Italy
(e-mail: matteo.corno@polimi.it, giulio.panzani@polimi.it,
sergio.savaresi@polimi.it)

Abstract: Solid-state LIDAR technology has recently emerged, allowing for smaller and more affordable devices. In the present work, we investigate the possibility of using a vehicle mounted solid-state LIDAR to estimate the vehicle pitch and heave dynamics. We present and compare two approaches: a model-based estimation and a data driven algorithm. The algorithms are tested on an instrumented vehicle. The experimental results show that the data-driven approach outperforms the model-based estimation in estimating pitch caused both by accelerations and braking and by road disturbances.

1. INTRODUCTION

Vehicle state estimation plays a key role in Vehicle Dynamics Control. Both industry and academia have dedicated considerable effort to vehicle state estimation with contributions on lateral dynamics (*i.e.* side slip), longitudinal (*i.e.* wheel slip) and vertical dynamics (*i.e.* pitch and heave). Examples of these systems can be found in Boniolo et al. (2009); Selmanaj et al. (2017); Busnelli et al. (2017); Bae et al. (2001); Grip et al. (2008).

Most estimation algorithms are designed to work with stock sensors: IMU's (inertial measurement units), wheel speed sensors. An example can be found in Oh and Choi (2013) where the vehicle roll and pitch angles are estimated based on measurements from a low-price six-dimensional IMU. The method relies on the combination of the velocity kinematics and the pseudo-integration of the angle kinematics and includes a cornering-stiffness adaptation scheme. In Tseng et al. (2007) a similar (IMU) measurement set-up is used. However, the authors propose two kinematics-based observer which are proven to be stable during cornering (i.e., vehicle yaw rate not zero). With an appropriate modeling, IMU data can be used to estimate the vehicle overall attitude as shown in Xiong et al. (2019), which includes pitch, roll, sideslip angles and vehicle velocity.

Alternative approaches integrate IMU and GPS measurements to improve estimate accuracy, example can be found in Wu et al. (2013); Bae et al. (2001); Ryu and Gerdes (2004).

Despite its maturity, the vehicle state estimation research field is still active and rich of challenges, as reported in Guo et al. (2018). Among the several, one of the most interesting is: "the range of vehicle dynamic state estimation must be extended towards automated and connected vehicles". Indeed, the recent introduction of advanced driver assistance systems (ADAS) leads to the addition of environmental sensors to the suite of commonly available sensors. The most common ones are cameras, radars and more recently LIDARs. Also these sensors can be integrated in the estimate. For example, Coulombeau and Laurgeau (2002); Labayrade and Aubert (2003); Kuyt and Corno (2018) consider the possibility of using cameras for vehicle state estimation.

LIDARs are the preferred sensors for autonomous driving because of their accuracy. They are often employed in navigation and localization. It is expected that LIDARs will become more and more common on vehicles as their cost drops. While they have been introduced for advanced autonomous localization and navigation purposes, their accuracy can be exploited also to improve more classical functionalities as vehicle state estimation.

In this paper, we design two vehicle pitch angle estimation algorithms. Both are based on LIDAR measurements; the first algorithm is a model based approach that assumes an ideal beam focused distance measurement. The second is black-box. A detailed analysis proves that the black-box approach yields better results as the beam focuse measurement hypothesis turns out not to be accurate for solid state LIDARs.

While not essential for safety systems, pitch angle estimation is useful for many vehicle dynamics control algorithms, for example suspension control. Active, or semi-active suspensions, along with an accurate knowledge of

the pitch, can be used to improve ride comfort. Similarly, an accurate estimation of the pitch angle could be useful to better adapt vehicle dynamics control to a varying static load distribution. One should also consider that estimating pitch angle by integrating the measurements from commercial grade IMU is not trivial because of the risk of drift.

The paper is organized as follows. In Section 2, the vehicle and LIDAR model is described. Section 3 introduces a white-box methods while Section 4 presents the black-box one. Section 5 shows the experimental results and the comparison of the methods. The paper ends with some concluding remarks.

2. PROBLEM SET UP AND DISCUSSION

This section clarifies the problem and the reference vehicle setup.

The solid state LIDAR used in this work is a LeddarVu8, a 2D solid state LiDAR by Leddartech. The LeddarVu8 uses a single fixed beam light source that is diffused over a field of view of 100 degrees. The total field of view is divided in detection segments: an array of photo-detectors that process the light reflected by objects in the field of view. In this research the device has been mounted vertically and the FoV (field of view) has been set to 36° divided in 6 segments. It is important to note that based on the workings of this technology, it is not possible to precisely pinpoint the direction of the detected object. It may lay every where in the sector. Despite this fact, we model each LIDAR segment as a single beam at the center of each sector. Figure 1 schematically represents the complete vehicle.
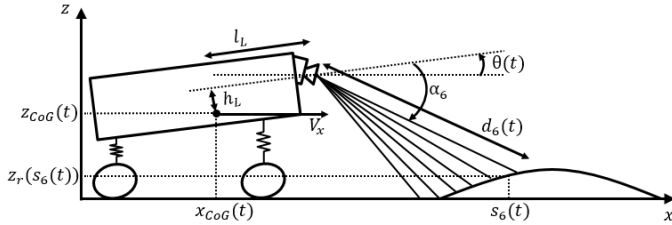

Fig. 1. LIDAR and vehicle model

The vehicle moves along the road at speed V_x, with pitch angle θ. The LIDAR is rigidly attached to the vehicle with a relative position with respect to the vehicle CoG represented by h_L and l_L. Each continuous line from the device to the road represents a LIDAR modeled segment. The i-th segment is measuring the distance $d_i(t)$ which varies in time, at the constant angle α_i. The latter is the angle between the modeled segment and the vehicle longitudinal axis. Quantities s_i and $z_r(s_i)$ are respectively the x and z coordinate of the road points measured by the i-th segment. The figure shows these quantities for segment 6. Quantities x_{CoG} and z_{CoG} are respectively the x and z coordinate of the vehicle CoG.

Given the above definitions, the absolute LIDAR position is determined by:

$$\begin{cases} x_L = x_{CoG} + l_L \cos(\theta) - h_L \sin(\theta) \\ z_L = z_{CoG} + l_L \sin(\theta) + h_L \cos(\theta) \end{cases} \quad (1)$$

and the x and z coordinates of the measured points are:

$$\begin{cases} s_i = x_L + d_i \cos(\alpha_i - \theta) \\ z_r(s_i) = z_L - d_i \sin(\alpha_i - \theta). \end{cases} \quad (2)$$

By substituting (1) into (2), one obtains:

$$\begin{cases} s_i = x_{CoG} + l_L \cos(\theta) - h_L \sin(\theta) + d_i \cos(\alpha_i - \theta) \\ z_r(s_i) = z_{CoG} + l_L \sin(\theta) + h_L \cos(\theta) - d_i \sin(\alpha_i - \theta). \end{cases}$$

From the last equation, an explicit expression for the measured distance d_i can be obtained:

$$d_i = \frac{z_{CoG} + l_L \sin(\theta) + h_L \cos(\theta) - z_r(s_i)}{\sin(\alpha_i - \theta)}. \quad (3)$$

The parameters h_L, l_L and α_i are constant and depend on the LIDAR placement.

Equation (3) points out that measured distances depend on three components: road surface, vehicle heave and vehicle pitch. In order to estimate vehicle quantities the following assumption is made. The assumption of driving on a flat surface yields:

$$z_r(s_i(t)) = 0 \ \forall s_i(t), \quad (4)$$

and (3) simplifies to:

$$d_i = \frac{z_{CoG} + l_L \sin(\theta) + h_L \cos(\theta)}{\sin(\alpha_i - \theta)}. \quad (5)$$

By defining the ratio $r_{i,j}$ as:

$$r_{i,j} = \frac{d_i}{d_j} = \frac{\sin(\alpha_j - \theta)}{\sin(\alpha_i - \theta)} \quad (6)$$

with $i \neq j$, one obtains an index that is not influenced by neither heave nor the LIDAR mounting position. In this case, there is a set of $n = 6$ elements (segments) which are combined into couples ($k = 2$), hence resulting in a total of $n_{ratios} = \frac{n!}{k! \cdot (n-k)!} = 15$ ratios. Each ratio is denoted as:

$$r_{i,j} \quad \text{where} \quad i = 1, 2, ..., 6 \ , \ j = 1, 2, ..., 6 \ \text{and} \ i < j. \quad (7)$$

Since α_i are constant and known, (6) represents a relation between ratios and pitch angle based on which the Pitch-Ratio Map of Figure 2 is obtained.
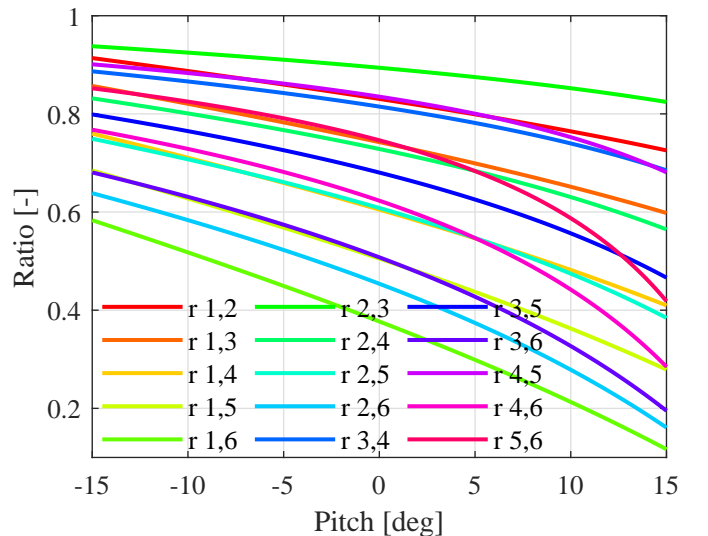

Fig. 2. Theoretical Pitch-Ratio Map as derived by the model.

3. WHITE-BOX RATIOS (WBR) ALGORITHM

As already pointed out, the distance ratios are independent from heave motions and, being α_i constant and known, are only influenced by pitch ones. Based on these observations, the following procedure is adopted in order to estimate the vehicle pitch and heave:

(1) Each ratio $r_{i,j}$ is used to obtain the estimate $\hat{\theta}_{i,j}$ through the Pitch-Ratio Map of Figure 2.

(2) The total estimate $\hat{\theta}$ is obtained as the mean of all $\hat{\theta}_{i,j}$:

$$\hat{\theta} = \frac{\sum_{i=1}^{n-1} \sum_{j=i+1}^{n} \hat{\theta}_{i,j}}{n_{ratios}} = \frac{\sum_{i=1}^{5} \sum_{j=i+1}^{6} \hat{\theta}_{i,j}}{15} \quad (8)$$

where n is the number of segments and n_{ratios} is the total number of ratios.

(3) Recalling (5), the estimated pitch $\hat{\theta}$ is used to produce heave estimates, one for each segment, as:

$$\widehat{z_{CoGi}} = d_i \sin(\alpha_i - \hat{\theta}) - l_L \sin(\hat{\theta}) - h_L \cos(\hat{\theta}) \quad (9)$$

(4) The total estimate $\widehat{z_{CoG}}$ is obtained as the mean of all $\widehat{z_{CoG\ i}}$:

$$\widehat{z_{CoG}} = \frac{\sum_{i=1}^{n} \widehat{z_{CoGi}}}{n} = \frac{\sum_{i=1}^{6} \widehat{z_{CoGi}}}{6} \quad (10)$$

4. BLACK-BOX RATIOS (BBR) ALGORITHM

In this section an alternative to the WBR estimation algorithm is presented.

In the model, the LIDAR is assumed to measure individual beams. In reality, each segment is 6° wide, and measurements are affected by noise and non-idealities. In order to account for the aforementioned effects a black-box approach is proposed.

The black-box approach is based on an experimental identification of the Pitch-Ratio map. Figure 3 plots the ratios obtained by comparing the LIDAR measurement against the pitch angle measured by a reference Inertial Measurement Unit. The figure also shows the modeled pitch-ratio map obtained by the model and a linear fitting of the experimental data. The figure mostly validates the first principle model with two important considerations:

- the identified lines are not exactly the ones predicted by the model but a linear fitting is nevertheless a good fitting for small θ.
- The ratios that include measurements from segment 1 appear to have an opposite slope with respect to what the model would predict. This could be due to the fact that the measurement does not refer to the center of the segment as hypothesized but to some other region of the sector.

Based on the above considerations, we propose the following linear black-box model of the pitch-ratio relation (valid for small θ):

$$r_{i,j} = m_{i,j} \cdot \theta + q_{i,j} \quad \text{for} \quad i=1,...,5, j=2,...6, i<j, \quad (11)$$

where the parameters $m_{i,j}$ and $q_{i,j}$ are identified through a least squares procedure.
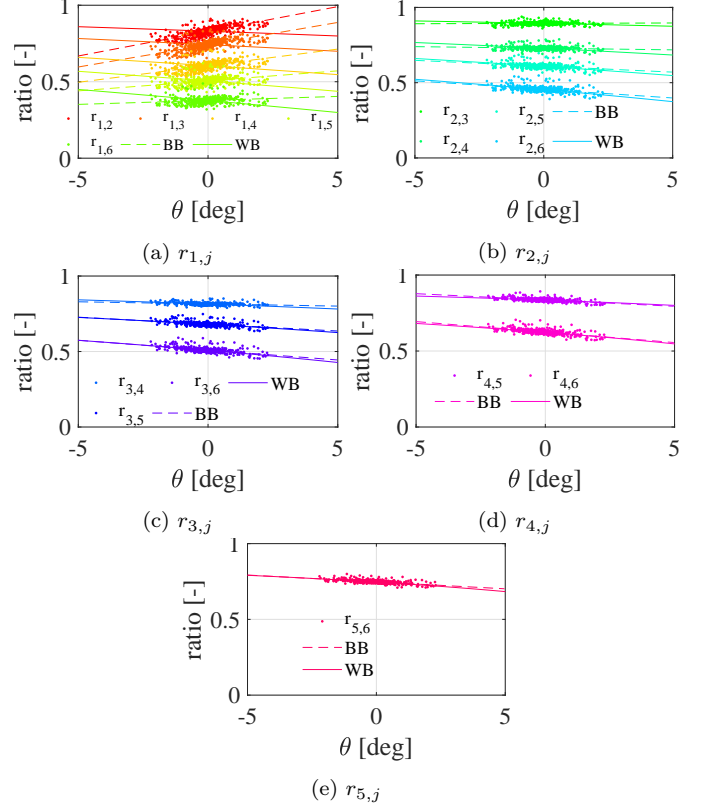

Fig. 3. Pitch-Ratio Map: black-box (BB) vs white-box (WB)

4.1 Ratio Informativeness Index - RII

In the ideal case, with perfect LIDAR measures, each ratio is useful for estimating the pitch angle. It is theoretically possible to have a perfect estimate of θ using only one ratio.

In reality noise and other phenomena affect the measures. The measurement errors affect different ratios differently. We assess the effect of noise and non idealities on each ratio with the Ratio Informativeness Index (RII). Recalling (11), the pitch at time k is estimated as:

$$\hat{\theta}_{i,j}(k) = \frac{r_{i,j}(k) - q_{i,j}}{m_{i,j}} \quad (12)$$

the estimation error is thus:

$$e_{i,j}(k) = \hat{\theta}_{i,j}(k) - \theta(k) \quad (13)$$

and leads to the following Ratio Informativeness Index as:

$$RII_{i,j} = \frac{abs(m_{i,j})}{\text{Var}(e_{i,j})}. \quad (14)$$

The Ratio Informativeness Index $RII_{i,j}$ gives an idea of how much information is contained in ratio $r_{i,j}$, i.e. how good the respective estimate $\hat{\theta}_{i,j}$ potentially is.

The index shows that the higher the slope, the more a pitch variation is observable from the ratio and therefore the better the noise and error rejection. In fact, for the same pitch variation, a higher slope causes a higher variation in the ratio, making noise and measurement errors less relevant. The error variance $\text{Var}(e_{i,j})$ is at the denominator. A large error variance means that the

identified line is badly fitting the data, therefore producing low quality estimates $\hat{\theta}_{i,j}$.

Figure 4 shows the $RII_{i,j}$ for the experimental data used for identification, where big differences among ratios are evident. As expected, ratios with almost zero slope (like $r_{2,3}$ and $r_{2,4}$) have a very low RII. On the other hand, ratios with high slopes (like $r_{1,2}$ and $r_{1,3}$) have a very high RII.
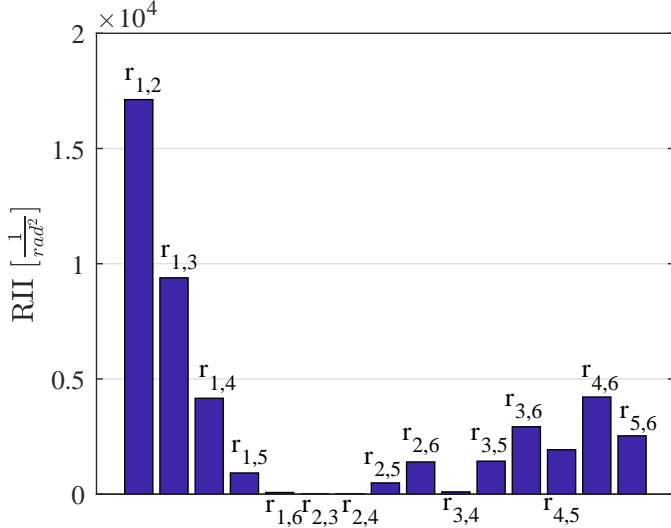

Fig. 4. RII for identification data

4.2 Black-Box Ratios reduced (BBRr) algorithm

Based on the results of the RII a reduced version of the BBR algorithm is here proposed, where only a subset of the $\hat{\theta}_{i,j}$ is used to produce the pitch estimate $\hat{\theta}_r$:

$$\hat{\theta}_r = \frac{\sum\limits_{(i,j)} \hat{\theta}_{i,j}}{8},\qquad(15)$$

where (i,j) are the ratios with the highest RII, i.e. $\{(1,2),(1,3),(1,4),(1,5),(3,6),(4,5),(4,6),(5,6)\}$.

5. EXPERIMENTAL RESULTS

The proposed methods are tested on experimental data and their results are compared.

The experimental set-up consists of a solid-state LIDAR, mounted on the front bumper of a Peugeot 206, which points towards the road. The vehicle is equipped with a high-end Inertial Measurement Unit (IMU) and a Global Positioning System (GPS) that provides, among other measures, the benchmark θ. Tests performed involve both hard accelerations and braking on a road without obstacles and driving over a speed bump.

The proposed methods are developed under the assumption of flat road profile. During the speed bump test this assumption is clearly not always true. A few seconds before the bump is hit the LIDAR will measure an obstacle. The algorithm needs to be aware of what is casing a variation in the LIDAR measurement. An IMU could be used to detect a vertical vehicle motion and activate the pitch

estimation algorithm; in this work we preliminary propose an algorithm that only uses the LIDAR measurement. To better understand the basic idea of the logic consider the scenario of a car driving up to a bump: the LIDAR will first *see* the bump and then it will hit it. During the phase in which the LIDAR is seeing the bump, the bump will be *sequentially* observed by each segment whereas during the bump hitting phase all sector will change at the same time. This information can be extracted by looking at the time derivative of the ratios. As each ratio actually considers two different segments, their derivative is expected to reach higher values when the LIDAR is detecting an obstacle on the ground. In this work, we set thresholds on the derivative of the ratio to activate the pitch angle estimation algorithm. Figure 5 shows the LIDAR distances
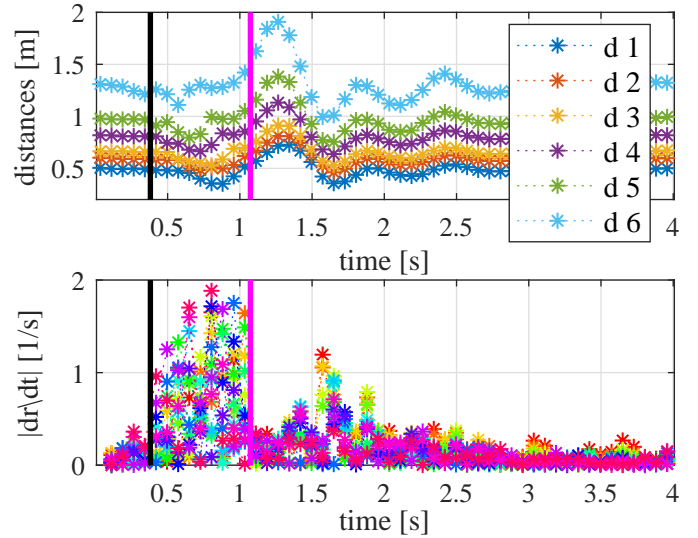

Fig. 5. LIDAR distances and the absolute value of the ratio time derivatives during a bump test. The vertical lines indicate the section where the pitch angle algorithm turns off and on.

and the absolute value of the ratio time derivatives during a bump test. The vertical lines indicate the section where the pitch angle algorithm turns off and on.

5.1 Speed bump test

Figure 6 plots the results of the pitch estimate over a speed bump. The figure plots the results of the three algorithms. One notices that out of the three algorithms, the black box using the reduced set of sensors is the one that provides the best results. The other two approaches wrongly estimates the amplitude and phase of the oscillations. To better understand the difference between the two algorithms, Figure 7 shows the estimated pitch angle for each ratio. In the WBR case, $\hat{\theta}_{1,2}$, $\hat{\theta}_{1,3}$ and $\hat{\theta}_{1,4}$ present a significant difference from the benchmark. Looking at the BBR instead, these components are much closer to θ. An explanation of this behavior is given by Figure 3a: if the BB line is considered as the true one (*i.e.*, identified from data), the WB line has a slope with an opposite sign, this causing the counter-phase behavior observed in Figure 7.

On the other hand, the BBR case presents some pitch estimates which are completely wrong: for example $\hat{\theta}_{3,4}$
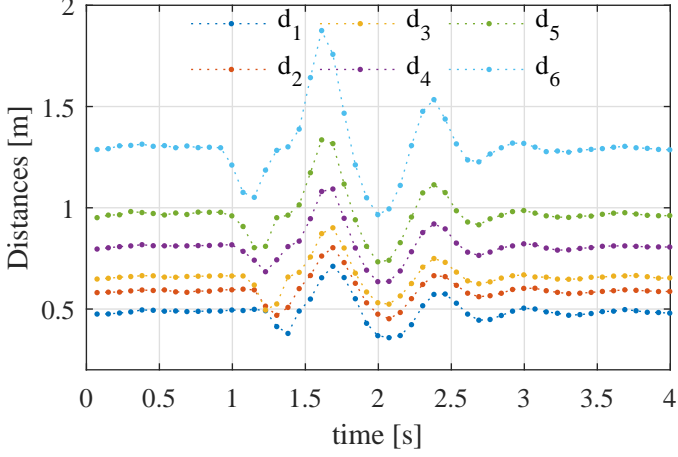
(a) LIDAR distances.
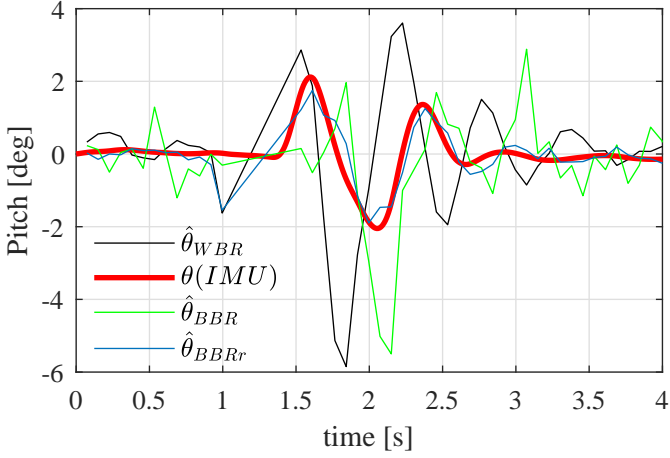
(b) Pitch estimate of the proposed algorithms and IMU.

Fig. 6. Experimental test over a speed bump.

which at $1.8\,\mathrm{s}$ is estimating around $-10°$, or at $\hat{\theta}_{2,3}$ which exceeds $\pm 15°$. This behaviour is expected, as these ratios are the ones with the lowest RII (Figure 4). Since the pitch-rate slopes related to these ratios are nearly zero, noise and measurements error have a big influence. This is confirmed by the superior performance obtained with the BBRr algorithm.

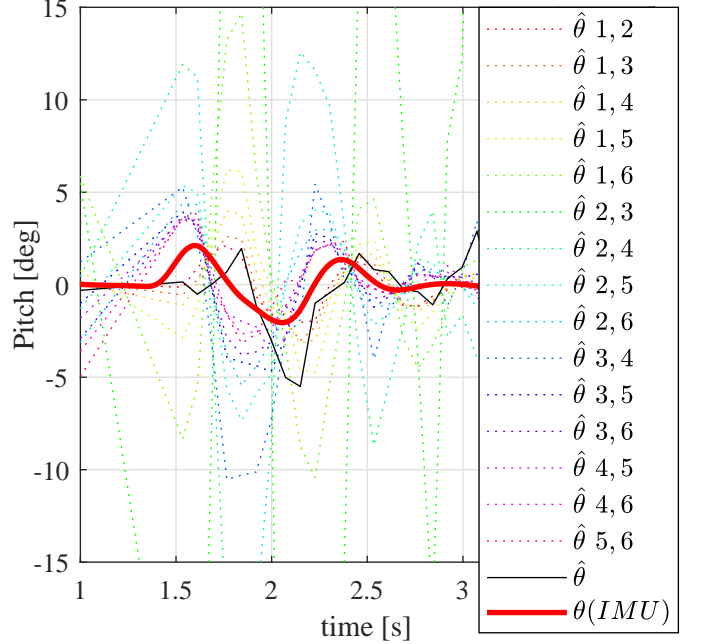### 5.2 Acceleration and braking test

Figure 8 plots the results during acceleration and braking. The results confirm the performance of the algorithm as analyzed during the speed bump test. The BBRr is the best algorithm among the proposed while the WBR is not shown due to its poor performance. Table 1 summarizes the estimation performance in terms of root mean square error (RMSE) of $\hat{\theta}$ with respect to the benchmark pitch θ.

5.3 Heave estimation

The LIDAR provides enough information to estimate the heave motion. The algorithm described in Section 3 is applied to the data using the pitch estimate obtained by the BBRr algorithm and Figure 9 plots the results for the speed bump data. The real heave coordinate is not available in the current experimental set-up, thus a formal
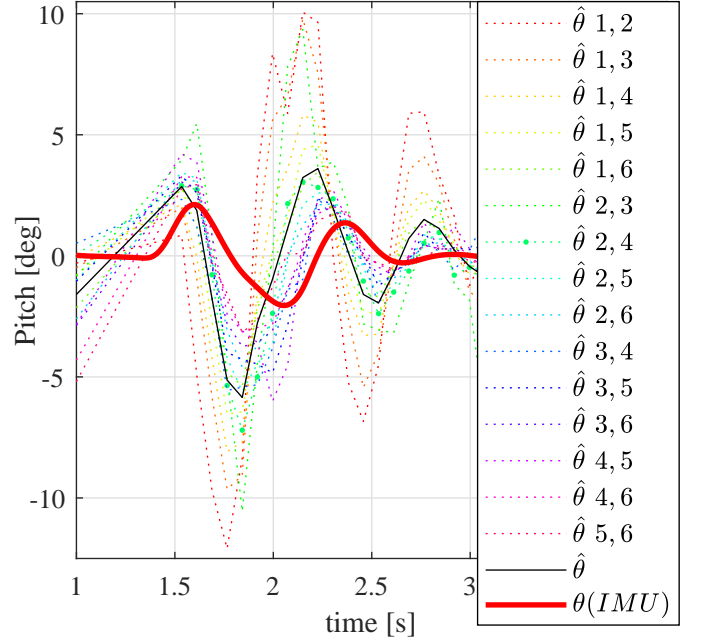
(a) WBR algorithm.

(b) BBR algorithm.

Fig. 7. Estimated pitch angle for all ratios.

Table 1. Mean square error (RMSE) results

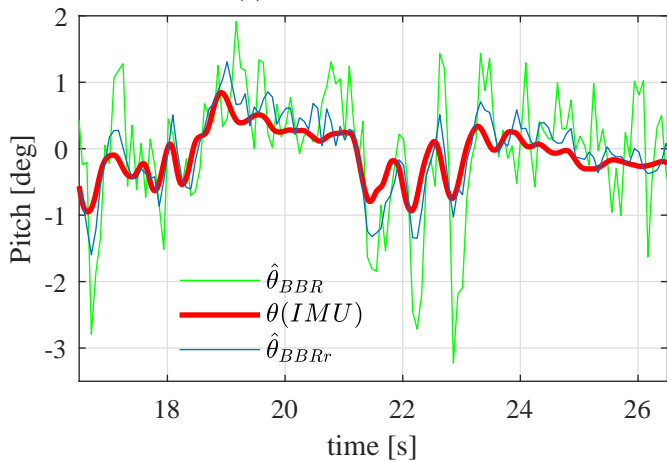| Algorithm	Speed bump	Acceleration and braking
WBR	1.60°	1.20°
BBR	1.18°	0.77°
BBRr	0.35°	0.29°

evaluation is not possible. However, the estimate shows a reasonable dynamics.

6. CONCLUSION

This paper studies the feasibility of a LIDAR based pitch dynamics estimation. We propose two methods to estimate
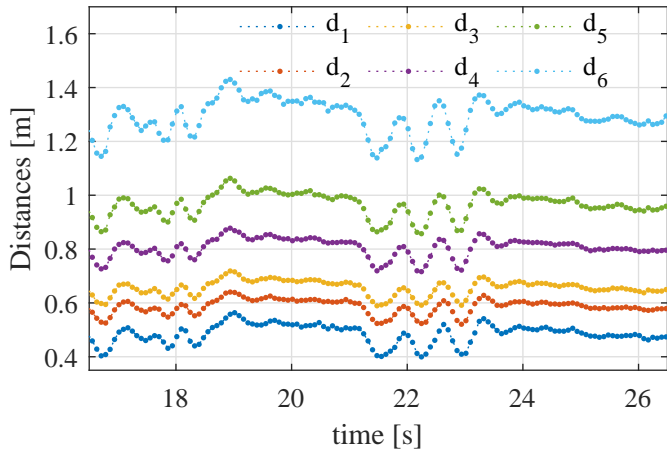
(a) LIDAR distances.

(b) Pitch estimate of BBR and BBRr algorithms and IMU.

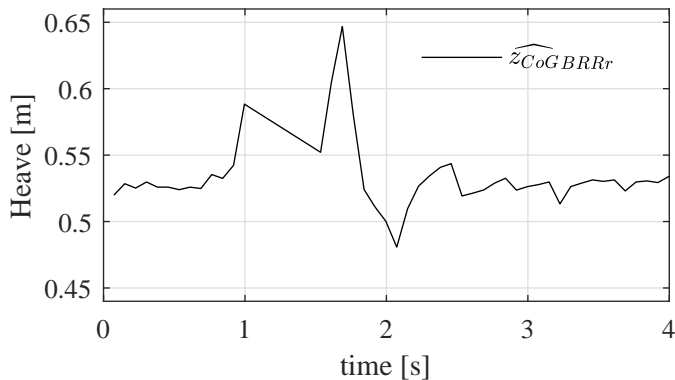Fig. 8. Acceleration and braking experimental test.

Fig. 9. BBRr heave estimation algorithm applied the speed bump experimental test of Figure 6a

the vehicle pitch angle based on a solid-state LIDAR. The first method uses a physical model of the vehicle and a simplified model of the LIDAR, while the second method exploits a black-box approach. The methods are tested and compared on experimental data showing that, given the specific features of the employed LIDAR, the black box approach yields better results.

A sensitivity analysis is also carried out and shows that not all the available LIDAR measurements provide sufficient signal-to-noise ratio to improve the pitch estimate. Based

on this analysis these measurements are excluded from the pitch estimation algorithm which improves significantly the estimate quality.

REFERENCES

Bae, H.S., Ryu, J., and Gerdes, J.C. (2001). Road grade and vehicle parameter estimation for longitudinal control using gps. In *Proceedings of the IEEE Conference on Intelligent Transportation Systems*, 25–29.

Boniolo, I., Savaresi, S., and Tanelli, M. (2009). Roll angle estimation in two-wheeled vehicles. *Control Theory & Applications, IET*, 3(1), 20–32.

Busnelli, F., Panzani, G., Corno, M., and Savaresi, S.M. (2017). Two-wheeled vehicles black-box sideslip angle estimation. In *2017 IEEE 56th Annual Conference on Decision and Control (CDC)*, 351–356.

Coulombeau, P. and Laurgeau, C. (2002). Vehicle yaw, pitch, roll and 3d lane shape recovery by vision. In *Intelligent Vehicle Symposium, 2002. IEEE*, volume 2, 619–625 vol.2.

Grip, H.F., Imsland, L., Johansen, T.A., Fossen, T.I., Kalkkuhl, J.C., and Suissa, A. (2008). Nonlinear vehicle side-slip estimation with friction adaptation. *Automatica*, 44(3), 611–622.

Guo, H., Cao, D., Chen, H., Lv, C., Wang, H., and Yang, S. (2018). Vehicle dynamic state estimation: state of the art schemes and perspectives. *IEEE/CAA Journal of Automatica Sinica*, 5(2), 418–431.

Kuyt, C. and Corno, M. (2018). Mixed kinematics and camera based vehicle dynamic sideslip estimation for an rc scaled model. In *2018 IEEE Conference on Control Technology and Applications (CCTA)*, 1216–1221. IEEE.

Labayrade, R. and Aubert, D. (2003). A single framework for vehicle roll, pitch, yaw estimation and obstacles detection by stereovision. In *IEEE IV2003 Intelligent Vehicles Symposium. Proceedings (Cat. No.03TH8683)*, 31–36.

Oh, J. and Choi, S.B. (2013). Vehicle roll and pitch angle estimation using a cost-effective six-dimensional inertial measurement unit. *Proceedings of the Institution of Mechanical Engineers, Part D: Journal of Automobile Engineering*, 227(4), 577–590.

Ryu, J. and Gerdes, J.C. (2004). Estimation of vehicle roll and road bank angle. In *Proceedings of the 2004 American Control Conference*, volume 3, 2110–2115.

Selmanaj, D., Corno, M., Panzani, G., and Savaresi, S. (2017). Vehicle sideslip estimation: A kinematic based approach. *Control Engineering Practice*, 67, 1 – 12.

Tseng, H.E., Xu, L., and Hrovat, D. (2007). Estimation of land vehicle roll and pitch angles. *Vehicle System Dynamics*, 45(5), 433–443.

Wu, Z., Yao, M., Ma, H., and Jia, W. (2013). Improving accuracy of the vehicle attitude estimation for low-cost ins/gps integration aided by the gps-measured course angle. *IEEE Transactions on Intelligent Transportation Systems*, 14(2), 553–564.

Xiong, L., Xia, X., Lu, Y., Liu, W., Gao, L., Song, S., Han, Y., and Yu, Z. (2019). Imu-based automated vehicle slip angle and attitude estimation aided by vehicle dynamics. *Sensors*, 19(8).